32

Probing Solution Thermodynamics by Microcalorimetry

Gregory M. K. Poon
Department of Pharmaceutical Sciences, Washington State University
U.S.A.

1. Introduction

Solution microcalorimetry has entrenched itself as a major technique in laboratories concerned with studying the thermodynamics of chemical systems. Recent developments in the calorimeter marketplace will undoubtedly continue to popularize microcalorimeters as mainstream instruments. The technology of microcalorimetry has in turn benefited from this trend in terms of enhanced sensitivity, signal stability, physical footprint and user-friendliness. As the popularity of solution microcalorimeters has grown, so has an impressive body of literature on various aspects of microcalorimetry, particularly with respect to biophysical characterizations. The focus of this chapter is on experimental and analytical aspects of solution microcalorimetry that are novel or represent potential pitfalls. It is hoped that this information will aid bench scientists in the formulation and numerical analysis of models that describe their particular experimental systems. This is a valuable skill, since frustrations often arise from uninformed reliance on turnkey software that accompany contemporary instruments. This chapter will cover both differential scanning calorimetry (DSC) and isothermal titration calorimetry (ITC). It targets physical chemists, biochemists, and chemical engineers who have some experience in calorimetric techniques as well as nonlinear regression (least-square analysis), and are interested in quantitative thermodynamic characterizations of noncovalent interactions in solution.

2. Differential scanning calorimetry

DSC measures the heat capacity (C_p) of a sample as the instrument "scans" up or down in temperature. For reversible systems, direct interpretation of the data in terms of thermodynamic parameters requires that chemical equilibrium be re-established much more rapidly than the scan rate. This can be verified by comparing data obtained at different scan rates. For transitions involving a change in molecularity (*e.g.*, self-association/dissociation, ligand binding/unbinding), reversibility can also be confirmed by the lack of hysteresis between heating and cooling experiments. The optimal scan rate is ultimately a compromise between the requirement for reversibility and the desire for reasonable throughput; typically this falls between 0.5 to 1.0 °C/min for most systems in dilute aqueous solutions.

2.1 Experimental conditions for DSC

The observed or apparent thermodynamics of solution systems generally include linked contributions from other solutes in addition to the species of interest. They include buffers,

salts, neutral cosolutes, and cosolvents. Of these, the choice of buffer, or any ionizable species in general, must take into account the change in pK_a with respect to temperature *i.e.*, the enthalpy of ionization (ΔH_{ion}). Unless a buffer's ΔH_{ion} is negligibly small, its pK_a will exhibit a temperature dependence, leading to a change in pH of the solution upon heating or cooling. Failure to take this fact into account may introduce significant artifacts into the observed melting behavior. Such changes in pH represent a different issue from any coupled ionization enthalpy arising from the release or uptake of protons associated with the transition of interest.

The direction and extent of the temperature of pH for a buffered solution depends on the sign and magnitude of ΔH_{ion} as well as the concentration of the buffering species. Consider the ionization of a buffer A^Z in the direction of deprotonation to produce its conjugate base B^{Z-1}:

$$A^z \rightleftharpoons B^{z-1} + H^+ \tag{1}$$

According to the van't Hoff equation,

$$\frac{dK_{ion}}{d(1/T)} = \frac{d10^{-pKa}}{d(1/T)} = -\frac{dH_{ion}}{R}, \tag{2}$$

where R is the gas constant, T is absolute temperature, and

$$K_{ion} = \frac{[H^+][B^{z-1}]}{[A^z]}. \tag{3}$$

Thus, for a buffer with a positive (endothermic) ΔH_{ion}, its ionization equilibrium shifts towards deprotonation as temperature increases, leading to a drop in pH. Conversely, the pH of a solution buffered by an exothermic buffer rises with increasing pH.

Table 1 lists several common buffers for aqueous solutions (King 1969; Disteche 1972; Lo Surdo et al. 1979; Kitamura and Itoh 1987; Goldberg et al. 2002). As a group, substituted ammonium compounds exhibit substantial positive values of ΔH_{ion}, making them poor choices for DSC experiments. These compounds include the so-called "Good buffers" (Good et al. 1966) that are prevalent in biochemistry. Among these, Tris, is a particular offender: the pH of a 25 mM solution initially buffered at pH 9.0 drops by more than one pH unit from 0 to 37°C (Poon et al. 2002). In contrast, the ionization of carboxylic acids and their analogues is far less sensitive to temperature. Generally, buffers based on acetate, cacodylate, and phosphate, for example, are preferred choices for DSC experiments.

Another important note relates to polyprotic species such as phosphates, citrates, and borates, whose pK_a also depends markedly on ionic strength. This relationship is quantitatively given by the volume changes of ionization ($\Delta V°$) and interpreted in terms of electrostriction of solvent water molecules. Thus, the addition of salts such as NaCl or guanidinium salts (the latter commonly used to denature proteins) will systematically reduce the pH of a solution buffered by polyprotic acids. The pH of a 0.1 M phosphate buffer at pH 7.2, for example, can fall by 0.5 pH unit upon addition of 0.5 M of NaCl. Molar concentrations of guanidinium hydrochloride will produce an even greater drop. On the other hand, inorganic cosolvents have the opposite effect by affecting the solution dielectric. Of course, once the pH of these buffers is adjusted to a value that is compatible with the apparent pK_a, it will be stable with respect to temperature. As seen in Table 1, it is generally the case that a buffer is either sensitive to temperature or ionic strength in aqueous solution.

Buffer	pK_a	$\Delta H°$, kJ mol^{-1}	$\Delta C_p°$, J K^{-1} mol^{-1}	$\Delta V°$, mL mol^{-1} [a]
Acetate	4.756	-0.41	-142	-10.6
Bicine	8.334	26.34	0	-2.0
Bis-tris	6.484	28.4	27	3.1
Cacodylate	6.28	-3	-86	-13.3
Citrate	3.128	4.07	-131	-10.7
	4.761	2.23	-178	-12.3
	6.396	-3.38	-254	-22.3
Glycine	2.351	4	-139	-6.8
	9.780	44.2	-57	
HEPES	7.564	20.4	47	4.8
Imidazole	6.993	36.64	-9	1.8
MES	6.27	14.8	5	3.9
MOPS	7.184	21.1	25	4.7
Phosphate	2.148	-8	-141	-16.3
	7.198	3.6	-230	-25.9
	12.35	16	-242	-36.0
Succinate	4.207	3.0	-121	
	5.636	-0.5	-217	
Tris	8.072	47.45	-142	4.3

[a] Ionization volume at atmospheric pressure at infinite dilution.

Table 1. Thermodynamic properties of ionization by common aqueous buffers

2.2 Analysis of DSC data

A complete DSC experiment consists of matched scans of a sample and a sample-free reference solution. Blank-subtracted data can be empirically analyzed to obtain model-independent thermodynamic parameters. The difference between pre- and post-transition baselines gives the change in heat capacity, ΔC_p. After subtracting a suitable baseline across the transition range, the arithmetic integration of the C_p vs. T trace yields the so-called calorimetric enthalpy:

$$\Delta H_{cal} = \int_{Ti}^{Tf} C_p dT \,. \tag{4}$$

ΔH_{cal} is the value of the transition enthalpy at the transition temperature, T_m. The entropy at T_m is

$$\Delta S(T_m) = \frac{\Delta H_{cal}}{T_m} \,. \tag{5}$$

Thus, a single DSC experiment yields the complete thermodynamics of a transition. Model-free determination of thermodynamics, including the direct measurement of ΔC_p, is a unique feature of DSC not possible with optical techniques (such as absorption and fluorescence spectroscopy) which access ΔH via the van't Hoff equation. However, model

fitting by least-square analysis can extract considerably more useful information and facilitate quantitative hypothesis testing.

In general, the reference-subtracted DSC data represent the heat capacity of the initial state 0 ($C_{p,0}$) as well as the excess heat capacity function, $\langle \Delta C_p(T) \rangle$:

$$C_p(T) = C_{p,0} + \left\langle \Delta C_p(T) \right\rangle . \tag{6}$$

Consider a general model in which the sample undergoes a transition from initial state 0 through intermediates 1, 2, ... , i to the final state n. (One can readily envisage extensions of this model in which a heterotypic complex dissociates into subunits which then go on to further, independent transitions.) The excess heat capacity function is (Privalov and Potekhin 1986)

$$\begin{aligned} \left\langle \Delta C_p(T) \right\rangle &= \frac{d\left\langle \Delta H(T) \right\rangle}{dT} = \frac{d}{dT}\left[\sum_{i=1}^{n} \Delta H_i(T)\alpha_i(T) \right] \\ &= \sum_{i=1}^{n} \Delta H_i \frac{d\alpha_i(T)}{dT} + \sum_{i=1}^{n} \alpha_i(T)\Delta C_{p,i} \\ &= \sum_{i=1}^{n} \left\langle \delta C_{p,i}^{tr}(T) \right\rangle + \sum_{i=1}^{n} \left\langle \delta C_{p,i}^{int}(T) \right\rangle \end{aligned} \quad , \tag{7}$$

where ΔH_i and $\Delta C_{p,i}$ are the enthalpy and heat capacity change, respectively, from state 0 to state i, and $\alpha_i(T)$ is the fractional conversion at state i. $\left\langle \delta C_{p,i}^{tr}(T) \right\rangle$ and $\left\langle \delta C_{p,i}^{int}(T) \right\rangle$ are called "transition" and "intrinsic" heat capacities, respectively. The intrinsic heat capacity, which represents the summed heat capacities of the various species present at T, is the baseline function of the observed DSC trace (Figure 1). Some analytical protocols invite the user to

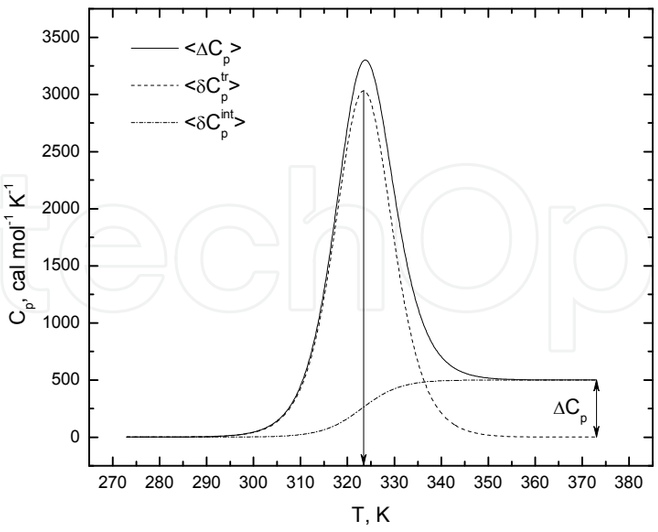

Fig. 1. An excess heat capacity function and its constituent transition and intrinsic heat capacities. Integration of the transition heat capacity, $\left\langle \delta C_{p,i}^{tr}(T) \right\rangle$, gives ΔH_{cal} at the transition temperature (50°C here).

perform manual baseline subtraction before fitting a excess heat capacity function. This is intended to eliminate $\left\langle \delta C_{\mathrm{p},i}^{\mathrm{int}}(T) \right\rangle$ from the fitting function. In the transition region, manual baseline subtraction requires either heuristic or semi-empirical criteria to connect the pre- and post-transitional states. This is both unnecessary and questionable practice, since manual editing may (and probably do) bias the data. The most appropriate approach is to fit both the excess and intrinsic heat capacities directly according to Eq (7). Since both terms are functions of $\alpha_i(T)$, the fitted baseline will objectively track the progress of each transition. Note that $C_{\mathrm{p},0}$ and $\Delta C_{\mathrm{p},i}$ are taken to be constants in Eqs (6) and (7) since their temperature dependence is generally weak over the experimental range. They can be formulated, if desired, as polynomials to define nonlinear baselines. Care must be taken, however, to ensure that such curvature is not masking some low-enthalpy transition such as conformation changes of proteins in the native state (Privalov and Dragan 2007).

2.2.1 Formulation of DSC models

The principal task in formulating DSC models is deriving expressions for $\alpha_i(T)$ from the relevant equilibrium expressions and equations of state. Implicit in this task is the computation of K_{i} from its corresponding thermodynamic parameters. This in turn requires the choice of a reference temperature, the most convenient of which is the characteristic temperature $T°$ at which $\Delta G(T°) = 0$:

$$\Delta G(T) = \Delta H(T°)\left(1 - \frac{T}{T°}\right) + \Delta C_{\mathrm{p}}\left(T - T° + T\ln\frac{T°}{T}\right). \tag{4}$$

Again ΔC_{p} is taken to be independent of temperature in the experimental range. The simplest DSC model involves the isomeric conversion of a species in a strictly two-state manner (*i.e.*, no intermediate state is populated at equilibrium). The denaturation of many single-domain proteins exemplifies this model. This excess heat capacity function is

$$\left\langle \Delta C_{\mathrm{p}}(T) \right\rangle = \frac{K}{(K+1)^2}\frac{\Delta H^2}{RT^2} + \frac{K}{K+1}\Delta C_{\mathrm{p}}\,. \tag{5}$$

The two terms on the right side represent $\left\langle \delta C_{\mathrm{p},i}^{\mathrm{tr}}(T) \right\rangle$ and $\left\langle \delta C_{\mathrm{p},i}^{\mathrm{int}}(T) \right\rangle$, respectively. The DSC traces in Figure 1 are simulated using Eq (5) with ΔH = 50 kcal/mol, ΔC_{p} = 500 cal mol^{-1} K^{-1}, and $T°$ = 50°C (1 cal ≡ 4.184 J). In this model, $T°$ is the midpoint of the transition (*i.e.*, K = 1 and $\alpha = \frac{K}{K+1} = 0.5$) and marks the maximum of the $\left\langle \delta C_{\mathrm{p},i}^{\mathrm{int}}(T) \right\rangle$ function.

For transitions involving changes in molecularity, $\alpha_i(T)$ includes total sample concentration, c_{t} in addition to equilibrium constants. While the mechanics of formulating such models is not different, a potential source of inconsistency arises from the choice of unit in thermodynamic parameters. Specifically, every intensive thermodynamic parameter can be defined either per unit of monomer or oligomer. Either choice is correct, of course, but the resultant differences may lead to some confusion. Take for example a two-state homo-oligomeric transition (Privalov and Potekhin 1986; Freire 1989):

$$X_n \underset{\rightleftharpoons}{\overset{K}{\rightleftharpoons}} nX\,, \tag{6}$$

where K is the equilibrium dissociation constant. Table 2 shows the subtle differences in accounting arising out of the two definitions.

Variable/parameter	Per unit monomer	Per unit oligomer
c_t	$[X] + n[X_n]$	$[X]/n + [X_n]$
α	$\frac{[X]}{c_t}$	$\frac{[X]}{nc_t}$
$\frac{d\alpha}{dT}$	$\frac{n\alpha(1-\alpha)}{n-\alpha(n-1)}\frac{\Delta H^2}{RT^2}$	$\frac{\alpha(1-\alpha)}{n-\alpha(n-1)}\frac{\Delta H^2}{RT^2}$
K	$nc_t^{n-1}\frac{\alpha^n}{1-\alpha}$	$n^n c_t^{n-1}\frac{\alpha^n}{1-\alpha}$
ΔG	$-nRT\ln K$	$-RT\ln K$

Table 2. Equivalent formulations of a two-state homo-oligomeric transition

In the author's experience (Poon et al. 2007), the choice of per unit monomer is more convenient, particularly when oligomers of different molecularities are compared. In addition, it can be seen that K is a polynomial in α of order n. Even in cases where α can be solved explicitly in terms of K and c_t ($n \leq 4$), it is advisable to use numerical procedures such as Newton's method instead to minimize potential algebraic errors and avoid a loss of significance in the fitting procedure.

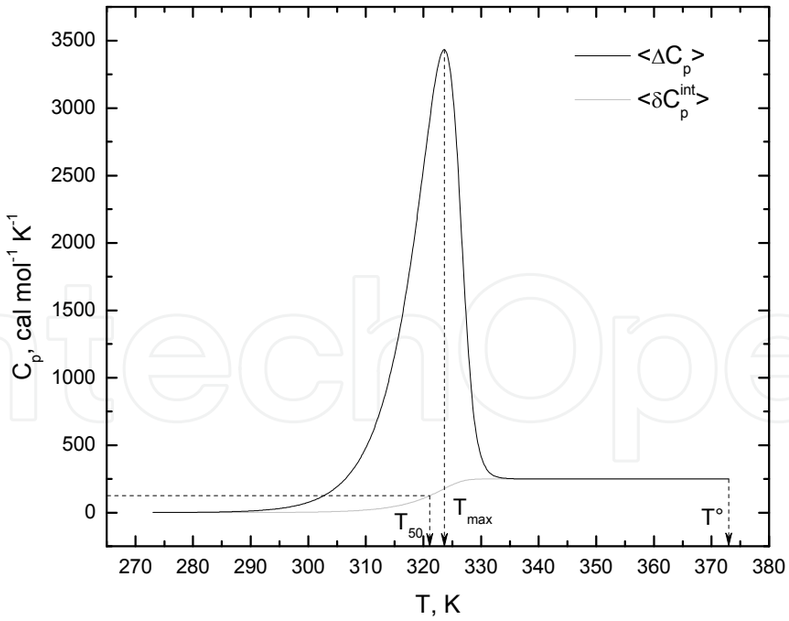

Fig. 2. Two-state dissociation of an homo-oligomer. The traces are simulated for a pentamer (n = 5) where ΔH = 50 kcal mol^{-1}, ΔC_p = 250 cal mol^{-1} K^{-1} and $T°$ = 100°C. All thermodynamics parameters are per unit *monomer*. Note the asymmetry in both heat capacity functions.

An additional consideration for transitions involving changes in molecularity concerns the choice and interpretation of the reference temperature. In contrast with isomeric transitions, $T°$ is neither the midpoint of a transition (in the context of concentrations) nor does it mark the maximum of the transition heat capacity function. Both of the latter temperatures are lower than $T°$. In addition, the midpoint of the transition, T_{50}, is below the temperature of the transition heat capacity maximum, T_m. These relationships are illustrated for the two-state dissociation model in Figure 2. The non-equivalence of T_m and T_{50} also introduces a systematic difference between the calorimetric and van't Hoff enthalpies (ΔH_{vH}, reported at T_m) (Freire 1989; Freire 1995). Moreover, the actual values of T_{50} and T_m are concentration-dependent, and this serves as a diagnostic for a change in molecularity in the transition. For data fitting purposes, $T°$ remains the most efficient choice because it is independent of concentration. After data fitting, estimates of T_m and T_{50} can also be easily obtained from the fitted curve.

Extension of the foregoing discussion applies readily to multi-state transitions. However, an explicit, statistical thermodynamic approach is generally used to derive the required equations for each state as a function of the partition function (Freire and Biltonen 1978). Details in deriving these models have been discussed extensively by Privalov's and Freire's groups (Privalov and Potekhin 1986; Freire 1994). From the standpoint of numerical analysis, it is worth noting that the excess enthalpy is the summed contributions from each state:

$$\left\langle \Delta C_p \right\rangle = \frac{d\left\langle \Delta H(T) \right\rangle}{dT} = \frac{d}{dT}\left[\sum_{i=1}^{n} \alpha_i(T) \Delta H_i(T) \right] \tag{7}$$

Depending on the number of states considered, the expansion of the derivative on the right side of Eq (7) can be formidable. Commercial programs such as Mathematica (Wolfram Research, Champaign, IL, USA) are thus recommended for symbolic manipulation for all but the most trivial derivations. Less preferably, one can numerically integrate the raw C_p vs. T data and fit $\left\langle \Delta H(T) \right\rangle$ directly. There are generally enough data points (at 0.1°C resolution) in an experiment that any loss of resolution should be negligibly small.

3. Isothermal titration calorimetry

As its name indicates, ITC measures the heat change accompanying the injection of a titrant into titrate at constant temperature. In contemporary instruments, this is accomplished by compensating for any temperature difference between the sample and reference cells (the latter lacking titrate, usually just water). The raw ITC signal is therefore power P, a time-dependent variable. Integration with respect to time therefore yields heat q which is the primary dependent variable that tracks the progress of the titration of interest:

$$q(\Delta t) = \int_0^{\Delta t} P dt \ . \tag{8}$$

Typically, ITC is operated in incremental mode in which the titrant is injected in preset aliquots after successive re-equilibration periods. A feature of ITC that distinguishes it from most titration techniques is that the measured heat does not accumulate from one injection to the next, but dissipates as the instrument measures the heat signal by returning the sample and reference cells to isothermal conditions. ITC is therefore a differential technique

with respect to the concentration of the titrant (X) *i.e.*, the derivative of q with respect to the total titrant concentration, $[X]_t$:

$$\frac{dq}{d[X]_t} = V\sum_{i=1}^{n}\Delta H_i \frac{d[X_i]_b}{d[X]_t}. \quad (9)$$

where $[X_i]_b$ is the concentration of X in the i-th bound state. This contrasts with most other physical binding signals (*e.g.*, absorbance, fluorescence intensity or anisotropy, pH) which are integrative in nature.

3.1 Experimental conditions for ITC

As a thermodynamic tool for studying molecular interactions, the singular strength of ITC is the direct measurement of binding enthalpies. Model-based analysis of ITC data, the subject of Section 3.2, allows the extraction of binding affinity and additional parameters in complex systems. As a label-free technique, ITC compares favorably with other titration techniques such as fluorescence and radioactivity. However, despite much-improved sensitivity (minimum detectable thermal energy <0.1 μJ), baseline stability, and titrant control found in contemporary instruments, sensitivity of ITC is relatively limited. The actual limit of detection depends primarily on the intrinsic enthalpy of the binding system at the temperature of interest, and to a lesser extent, the physical configuration of the instrument. Roughly speaking, a typical ITC experiment requires at least 10^{-6} M of titrate in a 1-mL volume and 10^{-4} M of titrant in a 100-μL syringe. (Recently, so-called "low volume" instruments equipped with 200-μL cells and 50-μL syringes have become available.)

The sensitivity of ITC is helped considerably by the differential nature of its signal (which is proportional to $\frac{dq}{d[X]_t}$) with respect to titrant concentration (Figure 3). In practice, the requirement for sufficient concentration in the sample cell to produce sufficient heat signals poses a direct limit on the tightest binding that may be reliably determined. Specifically, depletion of titrant dominates at titrate concentrations that are high relative to the dissociation constant K. Under this condition, the titration approaches a discontinuity in the first derivative at the equivalence point (Poon 2010). In the case of simple 1:1 binding, an empirical relationship that the product $1 < c_{titrate}/K < 1000$, where $c_{titrate}$ is the titrate concentration, is optimal for reliable estimation of K (Wiseman et al. 1989). One way of getting around this problem for very tight binding is to lower the apparent value of K by including a suitable, fixed concentration of competitor in the cell. Another possibility is continuous ITC, which will be discussed in Section 3.1.2. It should be noted that even under conditions where K cannot be determined, ΔH can still be determined by integration of the measured heat:

$$\Delta H = \frac{1}{c_{titrate}}\int_0^V \frac{q(v)}{v}dv, \quad (10)$$

where V is the volume of the (fixed) sample cell. (A volume correction is generally necessary; see Section 3.2.1.3.) A requirement for Eq (10) is, of course, that the titration is complete. Whichever the case, repeating the titration at different temperatures provides an estimate of the change in heat capacity by Kirchoff's relation:

$$\Delta C_{\mathrm{p}} = \frac{d\Delta H(T)}{dT} . \tag{11}$$

If the interaction under investigation occurs in a buffered solution, the earlier discussion on the temperature dependence of pK_a would again be relevant. More generally, binding that involves coupled uptake or release of protons will contain the buffer's enthalpy of ionization in the apparent binding enthalpy (Fisher and Singh 1995).

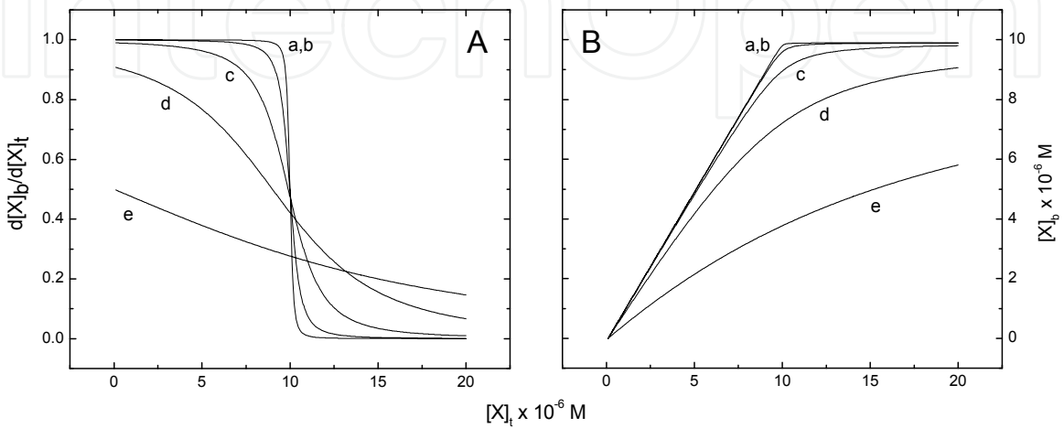

Fig. 3. The differential nature of ITC data. The volume and enthalpy are intentionally omitted to illustrate the differential nature of ITC data with respect to total titrant concentration. *S*imulated 1:1 binding to 10 μM titrate is shown in Panel *A*, with the corresponding integrated binding curves in Panel *B*. The values of *K* are as follows: a, 10^{-9} M; b, 10^{-8} M; c, 10^{-7} M; d, 10^{-6} M; and e, 10^{-5} M. The values of c_{titrate}/K range from 10^4 to 1.

Finally, ITC has been used as an "analog" of DSC for studying the stability of complexes. A concentrated solution of complex in the syringe is titrated into pure water or buffer in the cell. The resulting dilution drives complex dissociation and the attendant enthalpy is measured. This method has been used to characterize complexes through the spectrum of stoichiometries, from dimers (Burrows et al. 1994; Lovatt et al. 1996) to higher oligomers (Lassalle et al. 1998; Luke et al. 2005) to polymeric species (Stoesser and Gill 1967; Arnaud and Bouteiller 2004). Again, given the sensitivity of ITC, relatively high concentrations are required, so this technique is limited to the measurement of relatively weak complexes. It has been shown (Poon 2010) that the ITC data can be used to diagnose a dimeric or higher-order complex based on the presence of an inflection point in the latter.

3.1.1 Baseline signals

Two types of baselines are operative in an ITC experiment. One is instrument noise. Drifts on the order of 0.02 μW/h are routinely achievable in contemporary instruments. Another source of baseline arises from the injection of titrant. At the very least, viscous mixing makes a measurable if small exothermic contribution to the observed heat. This effect can be observed in a blank-to-blank injection (Figure 4), and serves as a casual useful indicator of the cleanliness of the cell and syringe between sample runs. Moreover, any mismatch in the matrices of the titrant and titrate will be manifest as a dilution enthalpy with each injection.

For small molecules, solids or lyophilized samples are usually dissolved in water or buffer. To complicate matters, hydrophobic solutes often require a cosolvent such as DMSO or DMF to achieve initial solubility before addition of the aqueous solvent; dilution of the cosolvent will therefore contribute to the observed heat at each injection. In other cases, ionizable solutes can perturb solution pH due to their substantial (>10^{-3} M) concentration in the syringe. Unless the solvent is adequately buffered, the pH in the cell and syringe will differ significantly and neutralization heats will contribute to the observed signal.

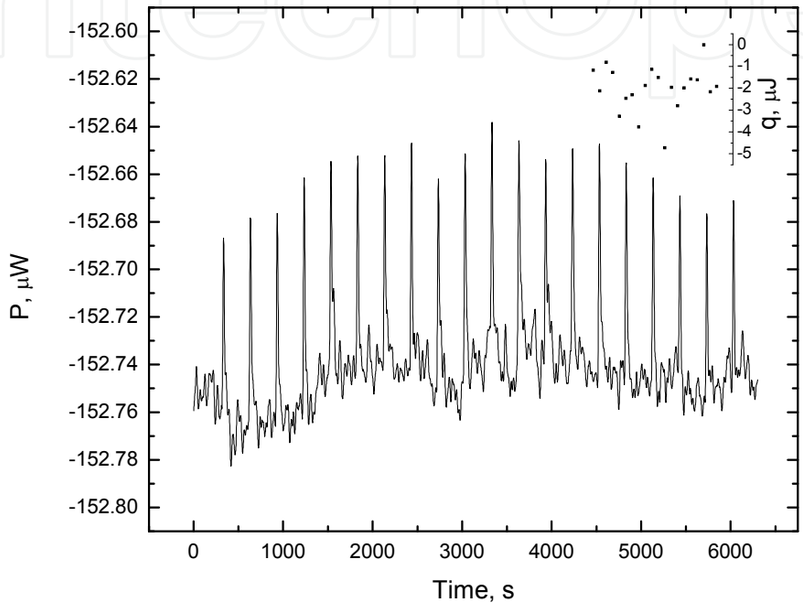

Fig. 4. Typical water-water control "titration." *Inset*, integrated areas of the water peaks. Given the low signal-to-noise ratios, the values must be considered very crude. However, the scatter also attests to the cleanliness of the cell and syringe.

In the case of macromolecular titrant and titrates, the solution matrices can be closely matched by extensive co-dialysis in the same solution. Care must be taken, however, with ionic polymers such as nucleic acids. These solutes can alter the distribution of ions in their compartment during dialysis due to the Donnan effect. Specifically, a non-diffusible polyionic solute excludes diffusible ions of the same charge from their compartment and therefore induces an asymmetric distribution of diffusible ions across the semipermeable membrane at equilibrium. To illustrate, for a simple system consisting only of the non-diffusible polyion M and a monovalent salt AB, the ratio concentrations of A^+ or B^- across the membrane is (Cantor and Schimmel 1980):

$$r_D = \frac{z[\mathrm{M}]}{2[\mathrm{AB}]_t} + \sqrt{1 + \left(\frac{z[\mathrm{M}]}{2[\mathrm{AB}]_t}\right)^2} \equiv \Psi + \sqrt{1 + \Psi^2}\ , \tag{12}$$

where z is the charge on the polyion (shown simply as M for brevity). At the concentrations required for the syringe, z[M] can be substantial. For example, a duplex oligonucleotide consisting of 20 base-pairs represents at 100 μM contributes 4 mM in total anions

(phosphates). The so-called Donnan ratio, r_D, is significantly above unity even at low polyion:salt ratios (Ψ). Eq (12) shows that a ten-fold excess of salt concentrations (Ψ=0.1) leads to a 10% exclusion of A or B from the compartment occupied by polyion. If AB is a buffer salt, the result is also a change of pH. Such asymmetry will modify the heat observed by ITC. As is well known, and illustrated by Eq (12), Donnan effects can be suppressed by ensuring a sufficient excess of diffusible salt in the dialysate. Unfortunately, the required salt concentrations may interfere with the investigation of interactions mediated substantially by electrostatic effects (as is usually the case for polyions). If possible, therefore, it is advisable to arrange for the polyionic species to be in the cell, where concentrations are lower.

In practical terms, none of these baselines effects are significant if the heat generated by the interaction of interest is sufficiently strong. This is not always achievable, however, for several reasons. Availability or solubility of the sample, particularly biological samples, may be limiting. It may also be desirable, for example, to perform titrations at a range of cell concentrations for binding to oligomerizing systems. Characterization of binding to a polyion at low salt concentration may require a reduced concentration. Thus, strategies for handling relatively low signal-to-noise situations are helpful in many situations. The most basic of these involve inspection and, where necessary, manual editing of the power baseline to mitigate the occasion excursion due to instrumental noise. To this end, an increase in the time between injection may be indicated to unambiguously identify the restoration of baseline. In addition, the residual heats (which may be up to 10 μJ) after the equivalence point are unlikely to be negligible. Subtraction with data from a titrant-to-blank run would likely introduce more noise into the data and be no more helpful than taking a simple average of the final post-equivalence heats. If the data is to be fitted to models, a more appropriate solution is to add a constant parameter *B* to the fitting equation:

$$\frac{dq_{\text{obsd}}}{d[\text{X}]_\text{t}} = V\sum_{i=1}^{n}\Delta H_i \frac{d[\text{X}_i]_\text{b}}{d[\text{X}]_\text{t}} + B\,. \tag{13}$$

3.1.2 Continuous ITC titrations

While incremental titrations most commonly performed in ITC, an alternative mode of operation is a continuous titration (cITC) (Markova and Hallén 2004). In cITC, the titrant is continuously into injected the cell at a low rate (~0.1 μL/s). The primary advantage of cITC is throughput. An incremental ITC experiment typically requiring 20 injections of 5 μL at intervals of 300 s takes (neglecting time for baseline stabilization) 100 min; at 0.1 μL/s, cITC would require approximately 17 min. Another potential motivation for cITC is increased resolution in terms of model-dependent analysis. In incremental ITC, peak-by-peak integration of thermal power is performed to obtain $\frac{dq}{d[\text{X}]_\text{t}}$. This step reduces the number of collected data points (typically 1 s^{-1} over 10^3 s, or about one to two hours) for nonlinear regression to the number of injections (usually 10 to 30). By using the thermal power data directly for fitting, cITC can in principle discriminate the curvature required to define tight binding.

Maintenance of quasi-equilibrium conditions throughout the titration is essential to correct interpretation of derived thermodynamic parameters and is a major concern for cITC. To this end, the stirring rate in cITC must be considerably increased (up to 700 rpm) relative to incremental ITC to facilitate mixing of titrant into the titrate solution. Additionally, the

instrument must be able to provide sufficient thermal compensation during the titration to maintain isothermal conditions. Finally, the kinetics of the interaction of interest must be fast relative to the injection rate. Generally speaking, these criteria are most likely met by relatively high-affinity interactions with moderate binding enthalpies.

3.2 Analysis of ITC data

The direct measurement of ΔH is considered a significant advantage over non-calorimetric binding methods since the latter access the binding thermodynamics indirectly in terms of the equilibrium constant K via the van't Hoff equation:

$$\frac{d\ln K}{d(1/T)} = -\frac{\Delta H_{\mathrm{vH}}}{R}. \tag{14}$$

Estimation of ΔC_{p} by non-calorimetric methods, therefore, involves taking a second derivative of the measured data. Another potential source of difficulty is the interpretation of K, which is model-dependent. As in DSC, however, ITC becomes a considerably more useful analytical technique when model fitting is used for parameter estimation and hypothesis testing. Moreover, agreement between the directly-fitted, calorimetric ΔH and the van't Hoff ΔH_{vH} obtained from Eq (14) is a strong indication of the physical correctness of the model at hand.

The most fundamental concept in the analysis of ITC data is the differential nature of the heat signal with respect to titrant concentration (Figure 3). Recalling Eq (9),

$$\frac{dq}{d[\mathrm{X}]_{\mathrm{t}}} = V\sum_{i=1}^{n}\Delta H_i \frac{d[\mathrm{X}_i]_{\mathrm{b}}}{d[\mathrm{X}]_{\mathrm{t}}}.$$

Integration of this fundamental equation gives the is the functional form of conventional binding models:

$$q([\mathrm{X}_i]_{\mathrm{b}}) = V\sum_{i=1}^{n}\Delta H_i[\mathrm{X}_i]_{\mathrm{b}}([\mathrm{X}_i]_{\mathrm{t}}) \tag{15}$$

The ideal approach to fitting ITC data is to directly fit Eq (9) (Poon 2010). For simple models, it is possible to write analytical expressions for $\frac{d[\mathrm{X}_i]_{\mathrm{b}}}{d[\mathrm{X}]_{\mathrm{t}}}$ explicitly in terms of $[\mathrm{X}]_{\mathrm{t}}$ i.e., the functional form of Eq (15). Take, for example, simple 1:1 binding of X + Y $\rightleftharpoons$ XY:

$$[\mathrm{X}]_{\mathrm{t}}[\mathrm{Y}]_{\mathrm{t}} - ([\mathrm{X}]_{\mathrm{t}} + [\mathrm{Y}]_{\mathrm{t}} + K)[\mathrm{X}]_{\mathrm{b}} + [\mathrm{X}]_{\mathrm{b}}^{\,2} = 0$$

$$[\mathrm{X}]_{\mathrm{b}} = \frac{[\mathrm{X}]_{\mathrm{t}} + [\mathrm{Y}]_{\mathrm{t}} + K - \sqrt{([\mathrm{X}]_{\mathrm{t}} + [\mathrm{Y}]_{\mathrm{t}} + K)^2 - 4[\mathrm{X}]_{\mathrm{t}}[\mathrm{Y}]_{\mathrm{t}}}}{2}, \tag{16}$$

where $K = \frac{[\mathrm{X}][\mathrm{Y}]}{[\mathrm{XY}]} = \frac{[\mathrm{X}][\mathrm{Y}]}{[\mathrm{X}]_{\mathrm{b}}}$ is the equilibrium dissociation constant. Its derivative is

$$\frac{d[\mathrm{X}]_{\mathrm{b}}}{d[\mathrm{X}]_{\mathrm{t}}} = \frac{1}{2} + \frac{1-\Phi-r}{2\sqrt{(\Phi+1+r)^2 - 4\Phi}}, \tag{17}$$

where $r = K/[X]_t$ and $\Phi = [X]_t/[Y]_t$. Eq (17) is sometimes referred to as the Wiseman isotherm (Wiseman et al. 1989). As complexity of the model increases, however, the algebra involved rapidly becomes prohibitive. In any case, numerical methods provide the means for generating solutions for Eq (9).

3.2.1 Numerical aspects of ITC data analysis

Given the usual practice of formulating models in terms of total or unbound concentrations, rather than their derivatives, conventional ITC data analysis has handled the differential nature of calorimetric data by fitting to a finite-difference version of Eq (9). Thus, for the *j*-th injection:

$$\Delta q_j = q_j - q_{j-1} - \delta q_j \,, \tag{18}$$

where δq_j is a volume-correction factor. This approach has the apparent advantage that models which have been formulated in terms of $[X]_b$ vs. $[X]_t$ can be used directly. However, Eq (18) represents poor practice in nonlinear regression. Since each computation of Δq_j requires evaluation of q corresponding to two consecutive injections, j and j-1, the data points (and their errors, albeit small) are not independent. Independence of observations constitutes a major assumption of nonlinear regression, one which the recursive form of Eq (18) clearly violates. Specifically, the residual in Δq_j during fitting becomes increasing correlated with increasing j. In addition, the resultant propagation of error likely violates the assumption of homoscedasticity (uniform variance) as well. Unless specialized regression techniques are employed (such as correlated least-squares), violations of these assumptions potentially calls the errors of the parameters, and possibly the parameters themselves, into question.

From the perspective of numerical analysis, Eq (18) is also entirely unnecessary. As stated previously, the most appropriate approach to handling ITC data is to fit Eq (9) directly. Posed in the form of Eq (9), ITC models (more specifically, the solution of $\frac{d[X]_b}{d[X]_t}$) represent classic initial value problems (IVPs). IVPs are first-order ordinary differential equations (ODEs) with a specific initial condition ($[X]_b = 0$ at $[X]_t = 0$) for which numerical methods for their solution are well-established. In addition avoiding the statistical pitfalls of Eq (18), formulating ITC models as differential equations simplify the algebra considerably. This is because implicit differentiation offers a welcome shortcut that obviates the need for an explicit solution for $[X]_b$. This is illustrated for $X + Y \rightleftharpoons XY$ with Eq (16):

$$\begin{aligned} [Y]_t - ([Y]_t + [X]_t + K)\frac{d[X]_b}{d[X]_t} - [X]_b + 2[X]_b\frac{d[X]_b}{d[X]_t} &= 0 \\ \frac{d[X]_b}{d[X]_t}(2[X]_b - [Y]_t - [X]_t - K) &= [X]_b - [Y]_t \\ \frac{d[X]_b}{d[X]_t} &= \frac{[X]_b - [Y]_t}{2[X]_b - [Y]_t - [X]_t - K} \end{aligned} \,. \tag{19}$$

Recognizing that $[X]_t$, $[Y]_t$ are constants (and K being the parameter to be estimated), Eq (19) takes on a noticeable simpler (but equivalent) form compared to the Wiseman isotherm, Eq (17). More importantly, implicit differentiation always yields an explicit ODE even when no

analytical expression for $[X]_b$ exists *e.g.*, polynomials of order >4. Direct substitution of Eq (19) into Eq (9) directly yields the ODE needed to generate values for nonlinear regression.
This approach of formulating explicit titration models for ITC has been demonstrated for many empirical models in common use, including the multi-site model, homotropic cooperativity, and two-state self-association (Poon 2010). To further illustrate the this approach, a competitive binding model will be examined. This is a method of measuring tight binding by ITC by adding a competitive species in the cell to reduce the apparent affinity (Sigurskjold 2000). The mechanism is an example of the general multi-site model involving two ligands competing for a single site (Wells 1992). The equilibrium distribution of bound titrate is a function of the affinities of the titrant X_1 and competitor X_2 for the titrate Y as well as the total concentrations of all three species. For the titrant-titrate complex, X_1Y:

$$a_0 + a_1[\mathrm{X_1Y}] + a_2[\mathrm{X_1Y}]^2 + a_3[\mathrm{X_1Y}]^3 = 0\,, \tag{20}$$

where

$$\begin{aligned} a_0 &= -K_2[\mathrm{X_1}]_\mathrm{t}^2[\mathrm{Y}]_\mathrm{t} \\ a_1 &= [\mathrm{X_1}]_\mathrm{t}\{K_1(K_2 + [\mathrm{X_2}]_\mathrm{t} - [\mathrm{Y}]_\mathrm{t}) + K_2([\mathrm{X_1}]_\mathrm{t} + 2[\mathrm{Y}]_\mathrm{t})\} \\ a_2 &= K_1^2 - K_2(2[\mathrm{X_1}]_\mathrm{t} + [\mathrm{Y}]_\mathrm{t}) - K_1(K_2 - [\mathrm{X_1}]_\mathrm{t} + [\mathrm{X_2}]_\mathrm{t} - [\mathrm{Y}]_\mathrm{t}) \\ a_3 &= K_2 - K_1 \end{aligned}$$

and K_1 and K_2 are the equilibrium dissociation constants of X_1 and X_2 for the titrate, respectively. The corresponding expression for the competitor-titrate complex, X_2Y, can be obtained from symmetry arguments:

$$b_0 + b_1[\mathrm{X_2Y}] + b_2[\mathrm{X_2Y}]^2 + b_3[\mathrm{X_2Y}]^3 = 0\,, \tag{21}$$

where

$$\begin{aligned} b_0 &= -K_1[\mathrm{X_2}]_\mathrm{t}^2[\mathrm{Y}]_\mathrm{t} \\ b_1 &= [\mathrm{X_2}]_\mathrm{t}\{K_2([\mathrm{X_1}]_\mathrm{t} - [\mathrm{Y}]_\mathrm{t}) + K_1(K_2 + [\mathrm{X_2}]_\mathrm{t} + 2[\mathrm{Y}]_\mathrm{t})\} \\ b_2 &= K_2(K_2 - [\mathrm{X_1}]_\mathrm{t} + [\mathrm{X_2}]_\mathrm{t} + [\mathrm{Y}]_\mathrm{t}) - K_1(K_2 + 2[\mathrm{X_2}]_\mathrm{t} + [\mathrm{Y}]_\mathrm{t}) \\ b_3 &= K_1 - K_2 \end{aligned}.$$

It is possible to solve the cubic equation in Eqs (20) and (21) explicitly, followed by differentiation of the solutions to obtain $\frac{d[\mathrm{X_1Y}]}{d[\mathrm{X_1}]_\mathrm{t}}$ and $\frac{d[\mathrm{X_2Y}]}{d[\mathrm{X_1}]_\mathrm{t}}$ as was done with the Wiseman isotherm. All of this is avoided, however, by implicit differentiation with respect to $[X_1]_t$ which directly yields the required derivatives:

$$\begin{aligned} \frac{d[\mathrm{X_1Y}]}{d[\mathrm{X_1}]_\mathrm{t}} &= \frac{-\left(\frac{da_2}{d[\mathrm{X_1}]_\mathrm{t}}[\mathrm{X_1Y}]^2 + \frac{da_1}{d[\mathrm{X_1}]_\mathrm{t}}[\mathrm{X_1Y}] + \frac{da_0}{d[\mathrm{X_1}]_\mathrm{t}}\right)}{3a_3[\mathrm{X_1Y}]^2 + 2a_2[\mathrm{X_1Y}] + a_1} \\ \frac{d[\mathrm{X_2Y}]}{d[\mathrm{X_1}]_\mathrm{t}} &= \frac{-\left(\frac{db_2}{d[\mathrm{X_1}]_\mathrm{t}}[\mathrm{X_2Y}]^2 + \frac{db_1}{d[\mathrm{X_1}]_\mathrm{t}}[\mathrm{X_2Y}] + \frac{db_0}{d[\mathrm{X_1}]_\mathrm{t}}\right)}{3b_3[\mathrm{X_2Y}]^2 + 2b_2[\mathrm{X_2Y}] + b_1} \end{aligned}. \tag{22}$$

The observed heat is now the sum of the enthalpy of unbinding of X_2 from Y and the binding of X_1 to Y:

$$\frac{dq}{d[\mathrm{X}]_\mathrm{t}} = V\left(\Delta H_{\mathrm{X1Y}}\frac{d[\mathrm{X_1Y}]}{d[\mathrm{X}_1]_\mathrm{t}} + \Delta H_{\mathrm{X2Y}}\frac{d[\mathrm{X_2Y}]}{d[\mathrm{X}_1]_\mathrm{t}}\right). \tag{23}$$

As shown in Figure 5, a judicious choice of competitor reduces the apparent affinity of the titrant to a range more amenable for regression. In this case, the initial condition for $[X_2Y]$ is *not* zero because the titrate is essentially pre-equilibrated with competitor before any titrant has been injected. The initial value for numerical integration is supplied by Eq (16):

$$[\mathrm{X_2Y}] = \frac{[\mathrm{X}_2]_\mathrm{t} + [\mathrm{Y}]_\mathrm{t} + K_2 - \sqrt{([\mathrm{X}_2]_\mathrm{t} + [\mathrm{Y}]_\mathrm{t} + K_2)^2 - 4[\mathrm{X}_2]_\mathrm{t}[\mathrm{Y}]_\mathrm{t}}}{2}.$$

Thus, the competitive model requires prior knowledge of both the concentration and affinity of the competitor. Since the competitor would therefore require its own characterization, a weak competitor is preferred, which means it would need to be present at significant concentrations (i.e., $[Y]_t \geq K$). Since binding of the titrate involves the unbinding of the competitor, the enthalpy of competitor unbinding may be substantially convoluted in the observed heat as indicated by Eq (23).

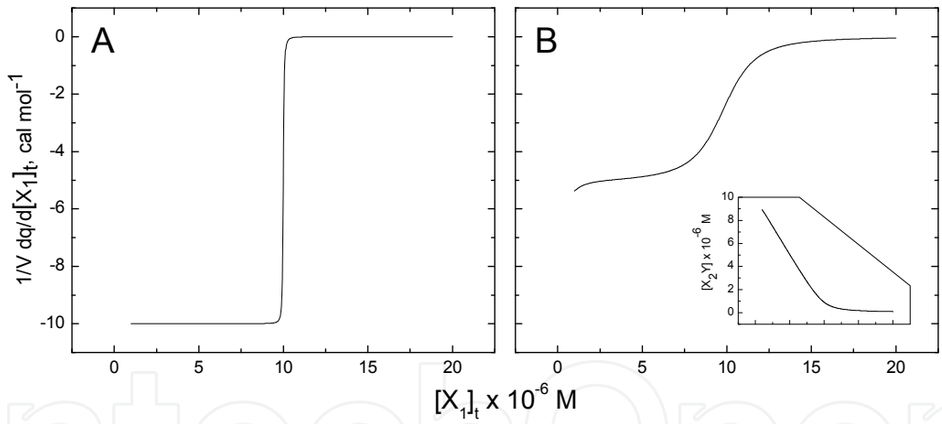

Fig. 5. Titrant-titrate binding in the presence of a competitor. *A*, simulated 1:1 titrant-titrate binding in the absence of competitor. The parameters are $K_1 = 10^{-10}$ M, $\Delta H_1 = -10$ kcal mol^{-1}, and $[Y]_t = 10$ μM. Data representing this level of affinity would be unfit for model-fitting; $K_1/[Y]_t = 10^4$. *B*, in the presence a competitor, X_2, at 10 μM ($K_2 = 10^{-8}$ M, $\Delta H_2 = -5$ kcal mol^{-1}). *Inset*, titration of the competitor.

Explicit titration models are also amenable to formulating models for continuous ITC. In the case of cITC, thermal power P is directly used in model fitting, so Eq (15) needs to be differentiated with respect to *time*:

$$P = \frac{dq(t)}{dt} = \frac{d}{dt}\left\{V\sum_{i=1}^{n}\Delta H_i[\mathrm{X}_i]_\mathrm{b}(t)\right\} = V\left[\sum_{i=1}^{n}\Delta H_i\frac{d[\mathrm{X}_i]_\mathrm{b}(t)}{dt}\right]. \tag{24}$$

Applying the chain rule and the relation $[\mathrm{X}_i]_{\mathrm{tot}} = \frac{c_{\mathrm{syr}} v_{\mathrm{inj}}}{V}$, where c_{syr} is the concentration of titrant in the syringe and v_{inj} is the injection volume,

$$\frac{d[\mathrm{X}_i]_{\mathrm{b}}}{dt} = \frac{d[\mathrm{X}_i]_{\mathrm{b}}}{d[\mathrm{X}_i]_{\mathrm{tot}}} \frac{d[\mathrm{X}_i]_{\mathrm{tot}}}{dt} = \frac{d[\mathrm{X}_i]_{\mathrm{b}}}{d[\mathrm{X}_i]_{\mathrm{tot}}} \left(\frac{c_{\mathrm{syr}}}{V} \frac{dv_{\mathrm{inj}}}{dt} \right). \tag{25}$$

(The subscript "tot" has been used to denote total concentration to avoid ambiguity with the variable t for time.) Note that $\frac{dv_{\mathrm{inj}}}{dt}$ is the (constant) injection rate. Substituting into Eq (24) gives

$$P = c_{\mathrm{syr}} \frac{dv_{\mathrm{inj}}}{dt} \left[\sum_{i=1}^{n} \Delta H_i \frac{d[\mathrm{X}_i]_{\mathrm{b}}}{d[\mathrm{X}_i]_{\mathrm{tot}}} \right]. \tag{26}$$

Thus explicit expressions of $\frac{d[\mathrm{X}_i]_{\mathrm{b}}}{d[\mathrm{X}_i]_{\mathrm{tot}}}$ can be directly used as in incremental ITC. At a sufficiently low injection rate, Eq (26) has the potential of "flattening out" the titration by transforming it in the time domain. This feature, in addition to the higher density of data points available for regression, may allow cITC to characterize much tighter binding than is practicable with incremental ITC (Markova and Hallén 2004).

In the foregoing discussion, the need to correct for various displacement and dilution effects due to the injection process has not been considered. In the author's experience, this is best handled during preliminary data reduction, before nonlinear regression. This aspect will be discussed in Section 3.2.1.3.

3.2.1.1 Choice of dependent variable

Another benefit of formulating ITC models as explicit ODEs is the flexibility in the choice of dependent variable for implicit differentiation, as long as it is a function in $[\mathrm{X}]_{\mathrm{t}}$. For the 1:1 binding model, formulation in terms of the unbound titrant X gives the (and simple) functional form of the familiar Langmuir isotherm:

$$[\mathrm{X}]_{\mathrm{b}} = \frac{[\mathrm{X}][\mathrm{Y}]_{\mathrm{t}}}{[\mathrm{X}] + K}. \tag{27}$$

Applying the chain rule of calculus,

$$\frac{d[\mathrm{X}]_{\mathrm{b}}}{d[\mathrm{X}]_{\mathrm{t}}} = \frac{d[\mathrm{X}]_{\mathrm{b}}}{d[\mathrm{X}]} \frac{d[\mathrm{X}]}{d[\mathrm{X}]_{\mathrm{t}}} = \frac{[\mathrm{X}]K}{([\mathrm{X}] + K)^2} \frac{d[\mathrm{X}]}{d[\mathrm{X}]_{\mathrm{t}}}. \tag{28}$$

At the same time, using the equation of state $[\mathrm{X}] = [\mathrm{X}]_{\mathrm{t}} - [\mathrm{X}]$,

$$\frac{d[\mathrm{X}]}{d[\mathrm{X}]_{\mathrm{t}}} = \frac{d([\mathrm{X}]_{\mathrm{t}} - [\mathrm{X}]_{\mathrm{b}})}{d[\mathrm{X}]_{\mathrm{t}}} = 1 - \frac{d[\mathrm{X}]_{\mathrm{b}}}{d[\mathrm{X}]_{\mathrm{t}}}. \tag{29}$$

Substituting the results from Eq (19) into Eq (29),

$$\frac{d[\mathrm{X}]}{d[\mathrm{X}]_t} = 1 - \frac{[\mathrm{X}]_b - [\mathrm{X}]_t}{2[\mathrm{X}]_b - [\mathrm{X}]_t - [\mathrm{Y}]_t - K} = \frac{[\mathrm{X}] + K}{2[\mathrm{X}] - [\mathrm{X}]_t + [\mathrm{Y}]_t + K} \tag{30}$$

The simultaneous equations (28) and (30) represent another formulation of the same model, except now [X] is the explicit dependent variable instead of $[X]_b$. (The initial condition is [X] = 0 at $[X]_t$ = 0.) Of course, we have previously derived Eq (19) directly, so this approach is regressive for this simple model. However, The flexibility to use any dependent variable of $[X]_t$ is useful, for example, for models that are formulated in terms of the binding polynomial which is based on [L] (Schellman 1975; Freire et al. 2009).

3.2.1.2 Practical considerations in implementing explicit ITC models

Successful implementation of Eq (9) requires numerical procedures for solving IVPs. The explicit, closed-form ODEs encountered in most models are typically ratios of polynomials. These functions are generally amenable any of the standard Runge-Kutta methods, which are widely available. A fast CPU is helpful, but not required. To this end, the tolerance for iteration should not be unnecessarily stringent in relation to the concentrations used and the value of *K* expected. Generally, a value of 10^{-6} will suffice. Even average single-core CPUs will handle ODEs of practical complexity with reasonable dispatch. Any significant delay is almost always related to input/output issues and can be alleviated by suppressing intermediate output. Numerical failures, if they occur, usually does so when there are two or more very different scales of the independent variable on which the dependent variable is changing *e.g.*, extremely tight binding to one site in the multi-site model. One such example is competitive binding in the presence of a very strong competitor in Eq (23). These pathological scenarios are associated with "stiff" differential equations that require more specialized algorithms for numerical solution. Fortunately, these situations are unlikely to be encountered as they are usually incompatible with experimental data in the first place.

Several technical software suites, such as Mathematica (Wolfram Research, Champaign, IL, USA), MATLAB (the MathWorks, Natick, MA USA), Maple (Maplesoft, Waterloo, Ontario, Canada), and IgorPro (WaveMetrics, OR, USA) which have built-in numerical ODE and least-square minimization capabilities, represent full-featured, integrated solutions. Alternatively, pre-compiled libraries containing optimized algorithms for numerical ODEs and least-square minimization are available commercially (the Numerical Algorithm Group Library; Numerical Algorithms Group [NAG], Oxford, UK) or free (GNU Scientific Library [GSL]) for most computing platforms. Functions from these libraries can be called under standard programming environments (*e.g.*, C/C++, FORTRAN) to perform the required procedures. Some commercial data analysis software such as Origin (Northampton, MA, USA) can interface with external libraries such as the NAG Library or GSL to perform numerical ODEs within their least-squares routines. If access to external libraries is not available, an adequate alternative is to code a numerical ODE algorithm (such as Runge-Kutta-Fehlberg) as part of the target function within the data fitting routines of the analysis program. "Cookbook" recipes for a variety of ODE solvers are straightforward and can be found in most texts of numerical analysis (Press 2007).

3.2.1.3 Volume correction

The sample and reference cells are typically overfilled for both DSC and ITC. Overfilling maximizes heat transfer between the solution and the wall of the cell as air is a poor thermal conductor. In the case of ITC, overfilling also minimizes stray signal arising from mechanical agitation of the solution-air-cell interface caused by the stirring paddle.

However, the introduction of titrant into an overfilled ITC sample cell leads to displacement effects that need to be taken into account. Specifically, each injected volume of titrant simultaneously displaces an equal volume of titrate and any previously injected titrant out of the sample cell (into the access tube). The accounting for these displaced volumes and their effect on titrant and titrate concentration is made on the assumption that the displaced material is immediately and completely excluded from the titration. This implies that no mixing occurs between the injected and displaced materials at the time injection. The concentrations of the titrant X after the *i*-th injection in the cell is therefore

$$[\mathrm{X}]_{\mathrm{t},i} = \frac{v_{\mathrm{inj}} c_{\mathrm{syr}} + [\mathrm{X}]_{\mathrm{t},i\text{-}1}(V - v_{\mathrm{inj}})}{V}, \quad [\mathrm{X}]_{\mathrm{t},0} = 0\,, \tag{4}$$

where V is the cell volume and v_{inj} is the injection volume. The corresponding concentrations of the titrate Y is

$$[\mathrm{Y}]_{\mathrm{t},i} = \frac{[\mathrm{Y}]_{\mathrm{t},i\text{-}1}(V - v_{\mathrm{inj}})}{V}\,. \tag{5}$$

There are two ways to handle volume corrections. One is to incorporate Eqs (4) and (5) as additional terms in the fitting equation. In the author's experience (Poon 2010), it is more efficient instead to perform the volume corrections on the dataset at the outset, and simply treat $[\mathrm{Y}]_{\mathrm{t},i}$ as an additional dependent variable in the least-square procedure.

3.2.1.4 Error analysis in ITC

Compared to other titrations, particularly in the biochemical laboratory, that requires extensive manual manipulation *e.g.*, electrophoretic mobility shift, filter binding, ITC instrumentation offers a greatly reduced level of statistical error in the measured data. Nonetheless, detailed theoretical and experimental studies of the nature and magnitude of statistical errors in ITC have offered insight into how instrumental errors can be minimized in fitted parameters. Although such studies have so far only focused on 1:1 binding, it has become clear that at least two régimes of instrumental errors exist (Tellinghuisen 2003; 2005b). Specifically, for titrations associated with relatively large heats (>300 μcal or "high-*q*"), proportional errors in the injected volumes dominate, and the inclusion of statistical weights is indicated to optimize fitted parameters. For "low-*q*" titrations, which typify low-concentration titrations needed for tight binding interactions, constant errors in thermal detection and compensation dominate, and unweighted fitting does not adversely affect parameter optimization. In either case, the optimal number of injections is considerably lower than the norm of 20 to 25 injections, especially if variable volume procedures are employed (Tellinghuisen 2005a). This approach could substantially reduce titration time and increase experimental throughput. It may be pointed out, however, that in some applications, sample-to-sample variation may be greater than any statistical error inherent in the analytical technique. In these cases, standard errors in parameters estimated from replicate experiments will be higher but more representative indicators of experimental uncertainty than the fitting error extracted from the variance-covariance matrix.

4. Conclusion

Commercial development of microcalorimetry has greatly increased the accessibility of this technique for the thermodynamic characterization of chemical systems in solution.

Unfortunately, the "black-box" nature of commercial software has engendered unwarranted reliance by many users on the turnkey software accompanying their instruments, and an attendant tendency to fit data to models of questionable relevance to the actual chemistry. This chapter discusses several novel aspects and potential pitfalls in the experimental practice and analysis of both DSC and ITC. This information should enable users to tailor their experiments and model-dependent analysis to the particular requirements.

5. Acknowledgement

Financial support by the College of Pharmacy at Washington State University is acknowledged.

6. References

Arnaud, A., and Bouteiller, L. (2004). Isothermal titration calorimetry of supramolecular polymers. *Langmuir* 20: 6858-6863

Burrows, S.D., Doyle, M.L., Murphy, K.P., Franklin, S.G., White, J.R., Brooks, I., McNulty, D.E., Scott, M.O., Knutson, J.R., and Porter, D. (1994). Determination of the monomer-dimer equilibrium of interleukin-8 reveals it is a monomer at physiological concentrations. *Biochemistry* 33: 12741-12745

Cantor, C.R., and Schimmel, P.R. (1980). *Biophysical Chemistry: the behavior of biological macromolecules*. W. H. Freeman, 0716711915, San Francisco, USA

Disteche, A. (1972). Effects of pressure on the dissociation of weak acids. *Symp Soc Exp Biol* 26: 27-60

Fisher, H.F., and Singh, N. (1995). Calorimetric methods for interpreting protein-ligand interactions. *Methods Enzymol* 259: 194-221

Freire, E. (1989). Statistical thermodynamic analysis of the heat capacity function associated with protein folding-unfolding transitions. *Comments Mol Cell Biophys* 6: 123-140

Freire, E. (1994). Statistical thermodynamic analysis of differential scanning calorimetry data: Structural deconvolution of heat capacity function of proteins. *Methods Enzymol* 240: 502-530

Freire, E. (1995). Thermal denaturation methods in the study of protein folding. *Methods Enzymol* 259: 144-168

Freire, E., and Biltonen, R.L. (1978). Statistical mechanical deconvolution of thermal transitions in macromolecules. I. Theory and application to homogeneous systems. *Biopolymers* 17: 463-479

Freire, E., Schön, A., and Velazquez-Campoy, A. (2009). Isothermal Titration Calorimetry: General Formalism Using Binding Polynomials. *Methods Enzymol* 455: 127-155

Goldberg, R.N., Kishore, N., and Lennen, R.M. (2002). Thermodynamic Quantities for the Ionization Reactions of Buffers. *J Phys Chem Ref Data* 31: 231-370

Good, N.E., Winget, G.D., Winter, W., Connolly, T.N., Izawa, S., and Singh, R.M.M. (1966). Hydrogen Ion Buffers for Biological Research. *Biochemistry* 5: 467-477

King, E.J. (1969). Volume changes for ionization of formic, acetic, and butyric acids and the glycinium ion in aqueous solution at 25°C. *J Phys Chem* 73: 1220-1232

Kitamura, Y., and Itoh, T. (1987). Reaction volume of protonic ionization for buffering agents. Prediction of pressure dependence of pH and pOH. *J Solution Chem* 16: 715-725

Lassalle, M.W., Hinz, H.J., Wenzel, H., Vlassi, M., Kokkinidis, M., and Cesareni, G. (1998). Dimer-to-tetramer transformation: loop excision dramatically alters structure and stability of the ROP four alpha-helix bundle protein. *J Mol Biol* 279: 987-1000

Lo Surdo, A., Bernstrom, K., Jonsson, C.A., and Millero, F.J. (1979). Molal volume and adiabatic compressibility of aqueous phosphate solutions at 25.degree.C. *J Phys Chem* 83: 1255-1262

Lovatt, M., Cooper, A., and Camilleri, P. (1996). Energetics of cyclodextrin-induced dissociation of insulin. *Eur Biophys J* 24: 354-357

Luke, K., Apiyo, D., and Wittung-Stafshede, P. (2005). Dissecting homo-heptamer thermodynamics by isothermal titration calorimetry: entropy-driven assembly of co-chaperonin protein 10. *Biophys J* 89: 3332-3336

Markova, N., and Hallén, D. (2004). The development of a continuous isothermal titration calorimetric method for equilibrium studies. *Anal Biochem* 331: 77-88

Poon, G.M. (2010). Explicit formulation of titration models for isothermal titration calorimetry. *Anal Biochem* 400: 229-236

Poon, G.M., Brokx, R.D., Sung, M., and Gariépy, J. (2007). Tandem Dimerization of the Human p53 Tetramerization Domain Stabilizes a Primary Dimer Intermediate and Dramatically Enhances its Oligomeric Stability. *J Mol Biol* 365: 1217-1231

Poon, G.M., Gross, P., and Macgregor, R.B., Jr. (2002). The sequence-specific association of the ETS domain of murine PU.1 with DNA exhibits unusual energetics. *Biochemistry* 41: 2361-2371

Press, W.H. (2007). *Numerical recipes : the art of scientific computing*, 3rd ed. Cambridge University Press, 0521880688, Cambridge, UK ; New York, USA

Privalov, P.L., and Dragan, A.I. (2007). Microcalorimetry of biological macromolecules. *Biophys Chem* 126: 16-24

Privalov, P.L., and Potekhin, S.A. (1986). Scanning microcalorimetry in studying temperature-induced changes in proteins. *Methods Enzymol* 131: 4-51

Schellman, J.A. (1975). Macromolecular binding. *Biopolymers* 14: 999-1018

Sigurskjold, B.W. (2000). Exact analysis of competition ligand binding by displacement isothermal titration calorimetry. *Anal Biochem* 277: 260-266

Stoesser, P.R., and Gill, S.J. (1967). Calorimetric study of self-association of 6-methylpurine in water. *J Phys Chem* 71: 564-567

Tellinghuisen, J. (2003). A study of statistical error in isothermal titration calorimetry. *Anal Biochem* 321: 79-88

Tellinghuisen, J. (2005a). Optimizing experimental parameters in isothermal titration calorimetry. *J Phys Chem B* 109: 20027-20035

Tellinghuisen, J. (2005b). Statistical error in isothermal titration calorimetry: variance function estimation from generalized least squares. *Anal Biochem* 343: 106-115

Wells, J.W. (1992). Analysis and interpretation of binding at equilibrium. In: *Receptor-Ligand Interactions: a Practical Approach.* E.C. Hulme(Ed., pp. 289-395. IRL Press at Oxford University Press, 0199630909, Oxford, England; New York, USA

Wiseman, T., Williston, S., Brandts, J.F., and Lin, L.N. (1989). Rapid measurement of binding constants and heats of binding using a new titration calorimeter. *Anal Biochem* 179: 131-137

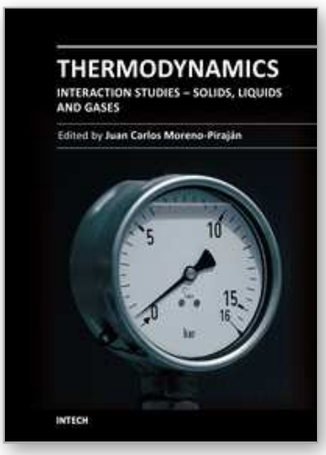

Thermodynamics - Interaction Studies - Solids, Liquids and Gases
Edited by Dr. Juan Carlos Moreno PirajÃ¡n

ISBN 978-953-307-563-1
Hard cover, 918 pages
Publisher InTech
Published online 02, November, 2011
Published in print edition November, 2011

Thermodynamics is one of the most exciting branches of physical chemistry which has greatly contributed to the modern science. Being concentrated on a wide range of applications of thermodynamics, this book gathers a series of contributions by the finest scientists in the world, gathered in an orderly manner. It can be used in post-graduate courses for students and as a reference book, as it is written in a language pleasing to the reader. It can also serve as a reference material for researchers to whom the thermodynamics is one of the area of interest.

How to reference
In order to correctly reference this scholarly work, feel free to copy and paste the following:

Gregory M. K. Poon (2011). Probing Solution Thermodynamics by Microcalorimetry, Thermodynamics - Interaction Studies - Solids, Liquids and Gases, Dr. Juan Carlos Moreno PirajÃ¡n (Ed.), ISBN: 978-953-307-563-1, InTech, Available from: http://www.intechopen.com/books/thermodynamics-interaction-studies-solids-liquids-and-gases/probing-solution-thermodynamics-by-microcalorimetry

INTECH
open science | open minds

InTech Europe
University Campus STeP Ri
Slavka Krautzeka 83/A
51000 Rijeka, Croatia
Phone: +385 (51) 770 447
Fax: +385 (51) 686 166
www.intechopen.com

InTech China
Unit 405, Office Block, Hotel Equatorial Shanghai
No.65, Yan An Road (West), Shanghai, 200040, China
中国上海市延安西路65号上海国际贵都大饭店办公楼405单元
Phone: +86-21-62489820
Fax: +86-21-62489821

IntechOpen